ACS OMEGA

http://pubs.acs.org/journal/acsodf

Article

Principal Component Analysis of Surface-Enhanced Raman Scattering Spectra Revealing Isomer-Dependent Electron Transport in Spiropyran Molecular Junctions: Implications for Nanoscale Molecular Electronics

Shuji Kobayashi, Satoshi Kaneko,* Takashi Tamaki, Manabu Kiguchi, Kazuhito Tsukagoshi, Jun Terao, and Tomoaki Nishino*

Cite This: *ACS Omega* 2022, 7, 5578−5583

Read Online

ACCESS | Metrics & More | Article Recommendations | Supporting Information

ABSTRACT: The characterization of single-molecule structures could provide significant insights into the operation mechanisms of functional devices. Structural transformation via isomerization has been extensively employed to implement device functionalities. Although single-molecule identification has recently been achieved using near-field spectroscopy, discrimination between isomeric forms remains challenging. Further, the structure−function relationship at the single-molecule scale remains unclear. Herein, we report the observation of the isomerization of spiropyran in a single-molecule junction (SMJ) using simultaneous surface-enhanced Raman scattering (SERS) and conductance measurements. SERS spectra were used to discriminate between isomers based on characteristic peaks. Moreover, conductance measurements, in conjunction with the principal component analysis of the SERS spectra, clearly showed the isomeric effect on the conductance of the SMJ.

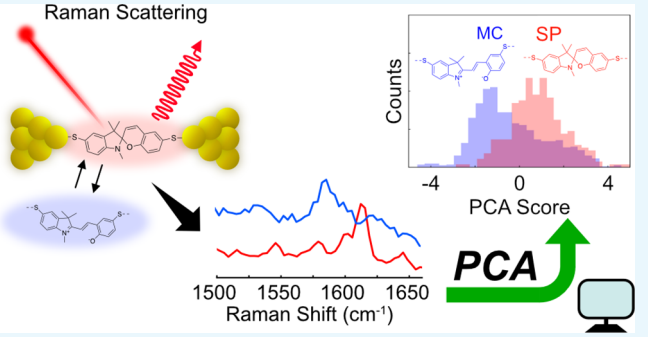

INTRODUCTION

Single-molecule studies have elucidated fundamental chemical processes such as catalytic reactions and mechanisms underlying device operation.[1,2] The identification of molecular structures provides critical clues for evaluating reaction mechanisms and the performance of devices composed of organic semiconductors. Surface-enhanced Raman scattering (SERS) is a promising means for the identification of single molecules, by taking advantage of the structural fingerprint of molecules in Raman spectra, without using chemical probes.[2−5] Meanwhile, recent developments in micro- and nanofabrication techniques have enabled the fabrication of single-molecule junctions (SMJs), wherein a single molecule bridges over a metal nanogap.[6,7] It has been demonstrated that SMJs are an ideal platform to investigate functionalities and physical phenomena at the single-molecule level. Recently, SERS has been applied to the observation of a single molecule in an SMJ, thereby enabling single-molecule identification.[8−15] However, relatively little experimental evidence has emerged regarding structural effects on the transport properties of an SMJ. We have thus developed SMJ SERS measurement techniques capable of the concurrent detection of electron transport, thereby revealing the interplay between structural and electronic properties.[11,12,16]

Structural changes in an SMJ are highly important because even minute changes, such as chemical transformations, changes in the adsorption state, or conformational changes of a molecule, can severely alter the electron transport properties.[6,7,16−18] This effect causes large fluctuations in the measured single-molecule conductance because the signals from individual molecules are directly detected in the single-molecule measurements, unlike in conventional ensemble measurements. The resulting dispersion in the data set hinders addressing the structure−function relationship, which necessitates a spectroscopic characterization simultaneously with conductance measurements. Despite the recent extensive efforts to observe SERS in SMJs, the detection of chemical transformations such as isomerization in an SMJ remains challenging. This difficulty arises because the spectral changes stemming from such a chemical transformation are indistinguishable from those caused by structural changes such as adsorption and conformational changes.[2,3]

Received: December 16, 2021
Accepted: January 19, 2022
Published: February 2, 2022

In the present study, we successfully identified the isomeric forms of a single molecule in an SMJ and revealed the intrinsic electronic properties of each isomeric form based on simultaneous SERS and current−voltage ($I-V$) measurements. Spiropyran (SP), which possesses advantageous photochromic characteristics associated with the isomerization between the SP and merocyanine (MC) forms,[19] was used to create the SMJ. Although the electrical switching of SP-SMJs owing to external stimuli can potentially be applied to fabricating molecular switches or memories,[20−22] the effect of isomerization on the alteration of electron transport properties remains unclear, and a multiparametric study is desirable to assess the isomeric effect. This is primarily because subtle changes in the conformation or adsorption sites of a molecule in an SMJ can significantly modulate the electrical conductance.[16,23] To overcome this problem, we first discriminate the two aforenoted isomers based on SERS. Principal component analysis (PCA)-based spectral analysis was performed on the SERS data for the extraction of SERS features from spectral fluctuations. Furthermore, $I-V$ responses acquired concurrently with SERS spectra revealed the electronic properties of each isomer, showing the underlying relationship between conductance and the molecular structure in diverse junction structures. The methodology proposed in this paper reveals the origin of electrical functionalities, which was difficult to assess via conventional SERS owing to spectral fluctuations. These findings will promote the establishment of optimal nanoscale systems for electronic devices or chemical catalysis.

EXPERIMENTAL SECTION

The electron transport and SERS measurements were performed using the mechanically controllable break junction (MCBJ) method (Figure 1a).[16,24,25] The electrode was fabricated using the following procedure. A 1 μm thick SiO_2 film was deposited on the polished 0.5 mm phosphor bronze substrate. The nanosized MCBJ electrode was fabricated using electron-beam lithography and the lift-off process. The narrowest structure of the electrode had dimensions of 300 nm × 150 nm with a thickness of 133.5 nm (Cr: 3.5 nm, Au: 130 nm). Free-standing Au nanobridges were fabricated using O_2 dry plasma etching. SP with two protected thiol groups (RS-SP-SR, R = 2-ethylhexyl-3-mercaptopropionate) was prepared following previously reported procedures[22] and deprotected immediately before the measurements. A tetrahydrofuran (THF)/ethanol/toluene solution of SP (1 mM) was drop-casted onto the electrode. Electron transport measurements were performed using a programmable amplifier (CA 5350, NF Corporation). First, the conductance of SP was determined using the MCBJ method. In this method, we repeated the formation and disconnection of the junction 4077 times at a frequency of 3 Hz under a bias voltage of 100 mV and constructed a conductance histogram based on the disconnecting process. SERS spectra were recorded using a NanoFinder 30A microscopic Raman spectrometer (Tokyo Instruments) with a 633 nm excitation laser. The laser beam was focused on the SMJs using a 50× objective lens. The Raman shift was calibrated with a symmetric vibrational mode of the Si single crystal observed at 520 cm^{-1}. The SERS spectra and $I-V$ response were continuously recorded in the conductance regime of the SMJs as determined by electron transport measurements. The trigger signal from the Raman spectrometer was recorded during the Raman measurement to correlate the Raman spectra with the $I-V$ response. The SERS spectra were recorded every 1 s. The bias voltage of the $I-V$ measurement was scanned between −1 and +1 V within 5 ms every 1 s. The number of traces was 156, which included 27 348 $I-V$ data points and SERS spectra. Of all the data, we analyzed 2135 data points and spectra that corresponded to at least two peak structures. We assigned the vibrational modes of the SP and MC forms by simulating the spectra of each form using Gaussian 16 with the B3LYP/6-31++G(d,p) method (Section 1 in the Supporting Information).

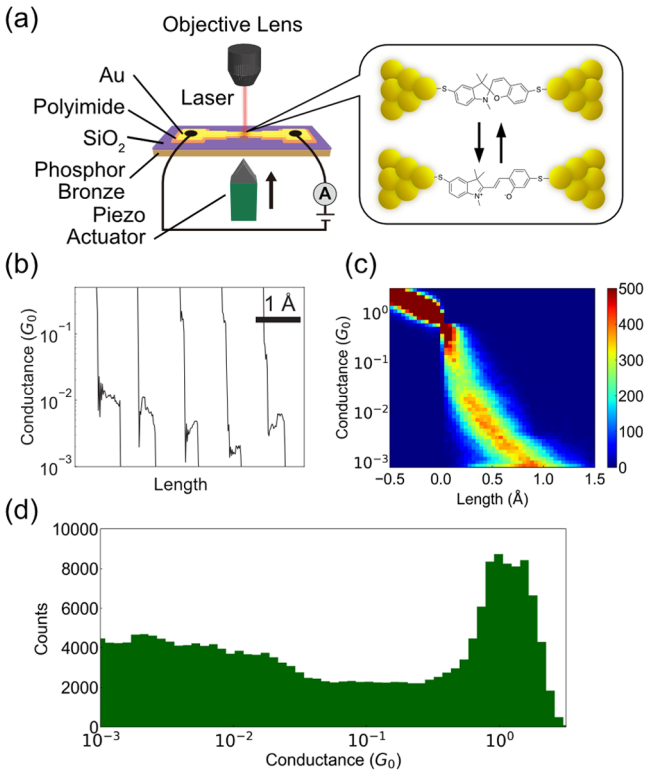

Figure 1. (a) Schematic of the experimental setup and conceptual image showing isomerization between spiropyran (SP) and merocyanine (MC). (b) Typical conductance trace of the break junction experiment for the SP single-molecule junction. (c) Two-dimensional (2D) conductance histogram. (d) One-dimensional (1D) conductance histogram. The bias voltage is 100 mV.

RESULTS AND DISCUSSION

The SMJ was fabricated using the mechanically controllable break junction (MCBJ) technique (Figure 1a). First, the conductance of the SP-SMJ was investigated by monitoring the conductance of the disconnection process without laser irradiation. Figure 1b shows the typical conductance−distance traces obtained during stretching in the MCBJ measurements. Each curve represents the change in conductance during the disconnection process of the gold electrodes in the presence of SP.[7,12,22,26] The plateaus in these traces indicate the formation of SMJs with stable structures.[26] The corresponding 2D and 1D histograms constructed using 4077 conductance traces (Figure 1c,d, respectively) show broadly distributed conductance states of the SMJs located within the 10^{-3}−10^{-2} G_0 region, which is consistent with the conductance of the SMJs of the SP and MC forms calculated in a previous study.[22] Because some traces, such as the 3rd−5th traces shown in Figure 1b, show abrupt changes during the plateau regions, the

https://doi.org/10.1021/acsomega.1c07105
ACS Omega 2022, 7, 5578−5583

isomerization might be induced during stretching, and the broad distribution in the conductance histograms in Figure 1c,d can be attributed to the isomerization effect owing to the mechanical stimuli and/or thermodynamic stabilization on the gold surface.[22,27] However, this discrimination is hampered by the conductance fluctuation originating from the variation in the configurations of the constituent molecules of the SMJ.[16,28] Notably, the conductance value obtained in the present study is greater than that reported in the previous study,[21,22] where the conductance was measured by the break junction (BJ) technique based on scanning tunneling microscopy (STM) measurements at 100 K. In the previously reported study, the authors focused on the low-conductive state just before the disconnection of the SMJ.[21,22] In the present study, the main focus is on the discrimination of the isomeric forms in the highly conductive region where discrimination has not been achieved solely by conductance measurements.[16,28]

To identify the two isomers and discriminate between these, SERS with simultaneous $I-V$ measurements was applied to the SMJs under the condition that the interelectrode distance of the SMJs was fixed. Figure 2a,b shows the SERS and $I-V$

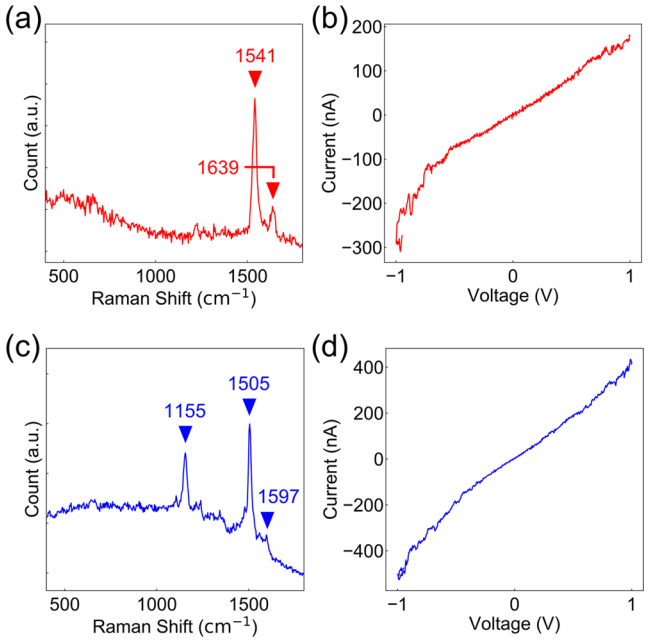

Figure 2. (a, b) Typical surface-enhanced Raman scattering (SERS) spectrum and current−voltage ($I-V$) curve of the single-molecule junction of the SP form. (c, d) Typical SERS and $I-V$ curve of the single-molecule junction of the MC form. Conductance values are 3.0 mG_0 (b) and 4.6 mG_0 (d).

response curves, respectively, obtained at a conductance value of 3 mG_0. In the SERS spectrum, a prominent peak is observed at 1541 cm^{-1}, accompanied by an additional peak at 1639 cm^{-1}. When similar measurements were performed at a conductance value of 4.6 mG_0 (Figure 2c,d), the prominent peak shifted to 1505 cm^{-1} and additional peaks were observed at 1155 and 1597 cm^{-1}.

The peaks observed for different conduction states were analyzed by comparing the spectra calculated by density functional theory (Section 1 in the Supporting Information) and the literature.[29−32] It was concluded that the SMJs in Figure 2a,c corresponded to the SP and MC forms, respectively (Section 2 in the Supporting Information). In the SP form (Figure 2a), the vibrations at 1541 and 1639 cm^{-1} were assigned to the C−C stretching vibration of the benzene ring in the benzopyran substructure and the C═C stretching vibration of the pyran ring, respectively. In the MC form (Figure 2c), the vibration at 1505 cm^{-1}, which originated from the cyclohexadiene ring, was assigned to the C−C and C═O stretching and C−H bending of the alkene substructure. The vibration at 1155 cm^{-1} was attributed to the ring breathing mode of the indole part. The peak at 1597 cm^{-1} was correlated to the C−C stretching vibration. We note that an SMJ is retained during the SERS measurements (Section 3 in the Supporting Information). Other examples of the $I-V$ response and SERS spectra are shown in Figure S5 (Section 4 in the Supporting Information). The asymmetric characteristics of the $I-V$ curve of SP are observed in Figure 2b. This behavior is consistent with the previous observations made by the STM-BJ measurements and is attributed to the energy-level shift due to the asymmetric molecular orbital.[22] In the present MCBJ studies, asymmetric $I-V$ curves were also obtained for the SMJ of the MC form, and the asymmetric geometries at the molecule/electrode interfaces[33,34] in addition to the aforementioned asymmetric orbital of SP are the possible origins of asymmetry. Notably, although SP was initially introduced in the electrode, the formation of the SMJs of both SP and MC was observed, which was attributed to the thermal isomerization of the MC form, as mentioned below.[19,27] The coexistence of the two isomers could be presumed from the conductance measured by the MCBJ technique (see above). The SERS spectra allow the identification of each isomer, as shown in Figure 2a,c. A combination of the vibrational characteristics of either SP or MC was utilized as a marker (Section 2 in the Supporting Information) to automatically classify all of the SERS spectra obtained in the current experiments. Based on the classification, the observation probabilities of the SP- and MC-SMJs were estimated to be 13 and 40%, respectively (Table S3). Notably, 47% of the measured spectra concurrently showed markers of SP and MC, which represented the time-averaged behavior of the ring-closing/opening reaction during spectral acquisition. The interconversion between the two isomers is evidenced by the synchronized signal between SERS and the $I-V$ response, as shown in Figure S6 (Section 5 in the Supporting Information). The preferable formation of the MC state was attributed to the thermodynamic stability of the isomers on the metal surface. According to the STM data obtained by Piantek et al., the MC form predominantly existed on the Au(111) surface at 300 K.[27] As MC is more conformationally flexible than SP, MC adopted a planar conjugated conformation upon adsorption, leading to the high stability of MC on the surface. In addition, the high dipole moment and hydrogen bond of zwitterions also stabilized the adsorbed states.[27] Thus, the SERS technique allowed the identification of MC and SP, revealing the populations of the two isomers, thereby reflecting their thermodynamic stabilities on the surface.

After successfully identifying SP and MC using the SERS data, the $I-V$ characteristics were analyzed to determine the effect of the molecular structures of the isomers on the electronic properties. The classifications by SERS were adapted to the simultaneously measured $I-V$ curves, and isomer-resolved conductance histograms were constructed (Figures 3a and S8 (Section 7 in the Supporting Information)). Although the histograms indicated the tendency of the MC-SMJ to show a higher conductance than the SP counterpart, the difference in

https://doi.org/10.1021/acsomega.1c07105
ACS Omega 2022, 7, 5578−5583

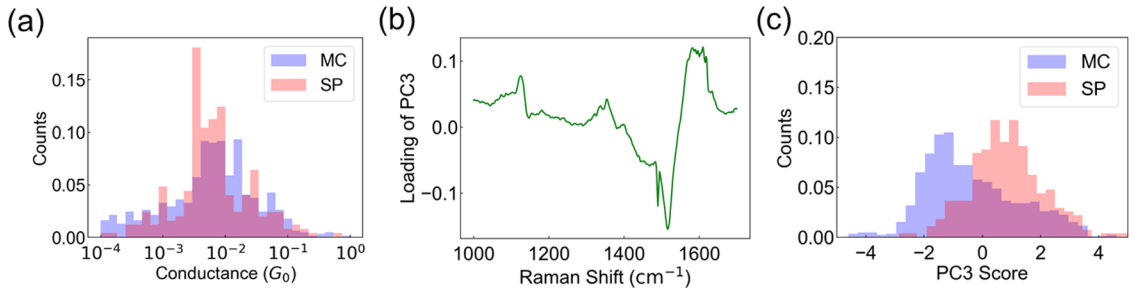

Figure 3. (a) Conductance histogram of the spiropyran (SP) single-molecule junction obtained by categorization based on the vibration mode of SERS spectra. (b) Loading of the 3rd principal component (PC3). (c) 1D histogram for the score of PC3. The red bar represents SP and the blue bar represents merocyanine (MC) in (a, b). The counts of the histogram were normalized by dividing by the total counts of each SP and MC form for (a, c), respectively.

the conductance between SP and MC was small compared to the distribution widths of the conductance histograms, which hampered the extraction of the intrinsic isomeric effects on the electronic properties. The minute fluctuations in the SM-SERS spectra, likely caused by structural changes without isomerization, inhibited the accurate identification of the isomers. The use of spectral features over the whole range, rather than the marker vibrations, can improve the accuracy of isomer assignment. Thereafter, the SERS spectra were analyzed using PCA to determine the relationship between the molecular structures of the isomers and conductance. PCA is a multivariate statistical analysis technique that can identify the major directions of variation in a given data set.[35−38] Intercorrelated quantitative dependent variables can be extracted from complex data by PCs.[38,39] Through the PCA of the SERS spectra, it was found that the third principal component (PC3) suitably reflected the isomerization behavior (Figure 3b,c), whereas PC1 and PC2 reflected the spectral background and the dominant MC isomer, respectively (Section 8 in the Supporting Information). The prominent peak at 1610 cm^{-1} in the loading vector of PC3, corresponding to the indole C−C stretching vibration of SP, is shown in Figure 3b, indicating that the discrimination between the SP- and MC-SMJs can be achieved via PC3.

To prove this, histograms of the PC3 scores for SP and MC, classified according to the vibrational modes (see above), were constructed (Figure 3c). Clearly distinct distribution was observed between SP and MC; the scores of SP and MC were distributed around +1.0 and −1.5, respectively. Thus, the isomeric form in the SMJs could be identified by PC3, and consequently, the relationship between the PC3 score, calculated using the SERS spectrum, and the conductance value, determined by the simultaneously acquired $I-V$ curve (Figure 4), could reveal the isomeric effects on the transport properties of the SMJs. The PC3−conductance 2D histogram shown in Figure 4 clearly exhibits anticorrelation and reveals that the MC-SMJ has a higher conductivity than SP-SMJ. This enhanced conductance value for MC is consistent with the previously reported conductance measurements.[20−22] The extended conjugation along the entire MC molecule induces a small energy gap between the Fermi energy and the conduction orbital.[20−22] Therefore, the PCA of SERS spectra characterized the conductance change due to isomerization, which is otherwise difficult to determine because of conductance fluctuation concomitant with the structural changes without isomerization. As previously described, SERS in conjunction with $I-V$ measurements is useful for chemical identification and investigation of the electronic

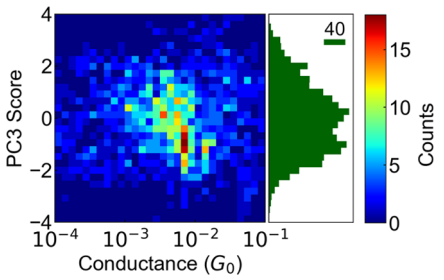

Figure 4. Two-dimensional histogram of the PC3 score and conductance. Data with conductance in the range of 10^{-4}−10^{-1} G_0 and score values ranging from −4 to 4 are displayed. The bin size for conductance and score value is defined by dividing each region into 30 parts.

properties of SMJs. The present study demonstrates that PCA in conjunction with SERS spectral analyses is a novel method to detect subtle chemical transformations such as the isomerization between SP and MC and investigate the relationship between the molecular structure and electronic properties, both of which are difficult to determine solely by conductance or spectroscopic measurements.

CONCLUSIONS

In this study, the SERS and $I-V$ properties of a thiol-anchored SP in an SMJ were investigated. The SERS spectra allowed the isomeric discrimination of the target molecule, which is generally difficult because of the conductance fluctuation of the SMJs. The relative populations of the SP and MC species were determined, which indicated their thermodynamic stability on the metal surface. Furthermore, PCA allowed the analysis of the SERS spectra based on the whole spectral features, as well as the correlation of the electron transport properties to the isomeric structures. The conductance dependence of the PC score highlighted the effect of the isomerization in the SMJs; the conductance of the MC form was higher than that of the SP form. SERS and electron transport measurements in conjunction with the PCA data can allow the determination of the effect of chemical transformations on the electrical properties of an SMJ.

ASSOCIATED CONTENT

Supporting Information

The Supporting Information is available free of charge at https://pubs.acs.org/doi/10.1021/acsomega.1c07105.

Details of the assignment of vibrational modes; analysis of SERS spectra; details of PCA; UV−visible absorption

https://doi.org/10.1021/acsomega.1c07105
ACS Omega 2022, 7, 5578−5583

spectrum of SP and the protonated MC form; and examples of observation of the ring-closing reaction (PDF)

AUTHOR INFORMATION

Corresponding Authors

Satoshi Kaneko − *Department of Chemistry, School of Science, Tokyo Institute of Technology, Tokyo 152-8551, Japan; JST PRESTO, Kawaguchi 332-0012, Japan;* orcid.org/0000-0002-0351-6681; Email: skaneko@chem.titech.ac.jp

Tomoaki Nishino − *Department of Chemistry, School of Science, Tokyo Institute of Technology, Tokyo 152-8551, Japan;* orcid.org/0000-0002-6691-5831; Email: tnishino@chem.titech.ac.jp

Authors

Shuji Kobayashi − *Department of Chemistry, School of Science, Tokyo Institute of Technology, Tokyo 152-8551, Japan*

Takashi Tamaki − *Department of Basic Science, Graduate School of Arts and Sciences, The University of Tokyo, Tokyo 153-8902, Japan;* Present Address: Department of Synthetic and Biological Chemistry, Graduate School of Engineering, Kyoto University, Kyotodaigakukatsura, Nishikyo-ku, Kyoto 615-8510, Japan

Manabu Kiguchi − *Department of Chemistry, School of Science, Tokyo Institute of Technology, Tokyo 152-8551, Japan;* orcid.org/0000-0002-8179-7466

Kazuhito Tsukagoshi − *International Center for Materials Nanoarchitectonics (WPI-MANA), National Institute for Materials Science (NIMS), Ibaraki 305-0044, Japan;* orcid.org/0000-0001-9710-2692

Jun Terao − *Department of Basic Science, Graduate School of Arts and Sciences, The University of Tokyo, Tokyo 153-8902, Japan;* orcid.org/0000-0003-1867-791X

Complete contact information is available at: https://pubs.acs.org/10.1021/acsomega.1c07105

Author Contributions

The manuscript was written through contributions of all authors. All authors have given approval to the final version of the manuscript. Satoshi Kaneko, K.T., M.K., and T.N. conceived and directed the experiments. Shuji Kobayashi and Satoshi Kaneko performed the measurements and analyzed the data. T.T. and J.T. synthesized the molecules.

Funding

This work was financially supported by a Grant-in-Aid for Scientific Research (20K05445, 21H01959), JSPS Fellowship (JP20J20661) from MEXT, and JST PRESTO (JPMJPR18I3).

Notes

The authors declare no competing financial interest.

ACKNOWLEDGMENTS

The numerical calculations were performed on a TSUBAME3.0 supercomputer at the Tokyo Institute of Technology, supported by the MEXT Project of the Tokyo Tech Academy for Convergence of Materials and Informatics (TAC-MI). The authors appreciate fruitful discussion with Dr. Yoichi Masui.

REFERENCES

(1) Zhang, J. L.; Zhong, J. Q.; Lin, J. D.; Hu, W. P.; Wu, K.; Xu, G. Q.; Wee, A. T. S.; Chen, W. Towards Single Molecule Switches. *Chem. Soc. Rev.* **2015**, *44*, 2998−3022.

(2) Choi, H.-K.; Lee, K. S.; Shin, H.-H.; Koo, J.-J.; Yeon, G. J.; Kim, Z. H. Single-Molecule Surface-Enhanced Raman Scattering as a Probe of Single-Molecule Surface Reactions: Promises and Current Challenges. *Acc. Chem. Res.* **2019**, *52*, 3008−3017.

(3) Yu, Y.; Xiao, T.-H.; Wu, Y.; Li, W.; Zeng, Q.-G.; Long, L.; Li, Z.-Y. Roadmap for Single-Molecule Surface-Enhanced Raman Spectroscopy. *Adv. Photonics* **2020**, *2*, No. 014002.

(4) Kneipp, J.; Kneipp, H.; Kneipp, K. SERS—a Single-Molecule and Nanoscale Tool for Bioanalytics. *Chem. Soc. Rev.* **2008**, *37*, 1052−1060.

(5) Nie, S.; Emory, S. R. Probing Single Molecules and Single Nanoparticles by Surface-Enhanced Raman Scattering. *Science* **1997**, *275*, 1102−1106.

(6) Aradhya, S. V.; Venkataraman, L. Single-Molecule Junctions Beyond Electronic Transport. *Nat. Nanotechnol.* **2013**, *8*, 399−410.

(7) Evers, F.; Korytár, R.; Tewari, S.; van Ruitenbeek, J. M. Advances and Challenges in Single-Molecule Electron Transport. *Rev. Mod. Phys.* **2020**, *92*, No. 035001.

(8) Liu, Z.; Ding, S.-Y.; Chen, Z.-B.; Wang, X.; Tian, J.-H.; Anema, J. R.; Zhou, X.-S.; Wu, D.-Y.; Mao, B.-W.; Xu, X.; Ren, B.; Tian, Z.-Q. Revealing the Molecular Structure of Single-Molecule Junctions in Different Conductance States by Fishing-Mode Tip-Enhanced Raman Spectroscopy. *Nat. Commun.* **2011**, *2*, No. 305.

(9) Konishi, T.; Kiguchi, M.; Takase, M.; Nagasawa, F.; Nabika, H.; Ikeda, K.; Uosaki, K.; Ueno, K.; Misawa, H.; Murakoshi, K. Single Molecule Dynamics at a Mechanically Controllable Break Junction in Solution at Room Temperature. *J. Am. Chem. Soc.* **2013**, *135*, 1009−1014.

(10) Tian, J.-H.; Liu, B.; Li, X.; Yang, Z.-L.; Ren, B.; Wu, S.-T.; Tao; Tian, Z.-Q. Study of Molecular Junctions with a Combined Surface-Enhanced Raman and Mechanically Controllable Break Junction Method. *J. Am. Chem. Soc.* **2006**, *128*, 14748−14749.

(11) Kaneko, S.; Murai, D.; Marqués-Gonzaléz, S.; Nakamura, H.; Komoto, Y.; Fujii, S.; Nishino, T.; Ikeda, K.; Tsukagoshi, K.; Kiguchi, M. Site-Selection in Single-Molecule Junction for Highly Reproducible Molecular Electronics. *J. Am. Chem. Soc.* **2016**, *138*, 1294−1300.

(12) Kobayashi, S.; Kaneko, S.; Kiguchi, M.; Tsukagoshi, K.; Nishino, T. Tolerance to Stretching in Thiol-Terminated Single-Molecule Junctions Characterized by Surface-Enhanced Raman Scattering. *J. Phys. Chem. Lett.* **2020**, *11*, 6712−6717.

(13) Kiguchi, M.; Aiba, A.; Fujii, S.; Kobayashi, S. Surface Enhanced Raman Scattering on Molecule Junction. *Appl. Mater. Today* **2019**, *14*, 76−83.

(14) Lee, J.; Crampton, K. T.; Tallarida, N.; Apkarian, V. A. Visualizing Vibrational Normal Modes of a Single Molecule with Atomically Confined Light. *Nature* **2019**, *568*, 78−82.

(15) Mahapatra, S.; Ning, Y.; Schultz, J. F.; Li, L.; Zhang, J. L.; Jiang, N. Angstrom Scale Chemical Analysis of Metal Supported Trans- and Cis-Regioisomers by Ultrahigh Vacuum Tip-Enhanced Raman Mapping. *Nano Lett.* **2019**, *19*, 3267−3272.

(16) Kaneko, S.; Montes, E.; Suzuki, S.; Fujii, S.; Nishino, T.; Tsukagoshi, K.; Ikeda, K.; Kano, H.; Nakamura, H.; Vázquez, H.; Kiguchi, M. Identifying the Molecular Adsorption Site of a Single Molecule Junction through Combined Raman and Conductance Studies. *Chem. Sci.* **2019**, *10*, 6261−6269.

(17) Xin, N.; Guan, J.; Zhou, C.; Chen, X.; Gu, C.; Li, Y.; Ratner, M. A.; Nitzan, A.; Stoddart, J. F.; Guo, X. Concepts in the Design and Engineering of Single-Molecule Electronic Devices. *Nat. Rev. Phys.* **2019**, *1*, 211−230.

(18) Kos, D.; Di Martino, G.; Boehmke, A.; de Nijs, B.; Berta, D.; Földes, T.; Sangtarash, S.; Rosta, E.; Sadeghi, H.; Baumberg, J. J. Optical Probes of Molecules as Nano-Mechanical Switches. *Nat. Commun.* **2020**, *11*, No. 5905.

(19) Klajn, R. Spiropyran-Based Dynamic Materials. *Chem. Soc. Rev.* **2014**, *43*, 148−184.

(20) Darwish, N.; Aragonès, A. C.; Darwish, T.; Ciampi, S.; Díez-Pérez, I. Multi-Responsive Photo- and Chemo-Electrical Single-Molecule Switches. *Nano Lett.* **2014**, *14*, 7064−7070.
(21) Walkey, M. C.; Peiris, C. R.; Ciampi, S.; Aragonès, A. C.; Domínguez-Espíndola, R. B.; Jago, D.; Pulbrook, T.; Skelton, B. W.; Sobolev, A. N.; Díez Pérez, I.; Piggott, M. J.; Koutsantonis, G. A.; Darwish, N. Chemically and Mechanically Controlled Single-Molecule Switches Using Spiropyrans. *ACS Appl. Mater. Interfaces* **2019**, *11*, 36886−36894.
(22) Tamaki, T.; Minode, K.; Numai, Y.; Ohto, T.; Yamada, R.; Masai, H.; Tada, H.; Terao, J. Mechanical Switching of Current−Voltage Characteristics in Spiropyran Single-Molecule Junctions. *Nanoscale* **2020**, *12*, 7527−7531.
(23) Kim, T.; Darancet, P.; Widawsky, J. R.; Kotiuga, M.; Quek, S. Y.; Neaton, J. B.; Venkataraman, L. Determination of Energy Level Alignment and Coupling Strength in 4,4′-Bipyridine Single-Molecule Junctions. *Nano Lett.* **2014**, *14*, 794−798.
(24) Kobayashi, S.; Kaneko, S.; Fujii, S.; Nishino, T.; Tsukagoshi, K.; Kiguchi, M. Stretch Dependent Electronic Structure and Vibrational Energy of the Bipyridine Single Molecule Junction. *Phys. Chem. Chem. Phys.* **2019**, *21*, 16910−16913.
(25) van Ruitenbeek, J. M.; Alvarez, A.; Piñeyro, I.; Grahmann, C.; Joyez, P.; Devoret, M. H.; Esteve, D.; Urbina, C. Adjustable Nanofabricated Atomic Size Contacts. *Rev. Sci. Instrum.* **1996**, *67*, 108−111.
(26) Xu, B.; Tao, N. J. Measurement of Single-Molecule Resistance by Repeated Formation of Molecular Junctions. *Science* **2003**, *301*, 1221−1223.
(27) Piantek, M.; Schulze, G.; Koch, M.; Franke, K. J.; Leyssner, F.; Krüger, A.; Navío, C.; Miguel, J.; Bernien, M.; Wolf, M.; Kuch, W.; Tegeder, P.; Pascual, J. I. Reversing the Thermal Stability of a Molecular Switch on a Gold Surface: Ring-Opening Reaction of Nitrospiropyran. *J. Am. Chem. Soc.* **2009**, *131*, 12729−12735.
(28) Kim, Y.; Pietsch, T.; Erbe, A.; Belzig, W.; Scheer, E. Benzenedithiol: A Broad-Range Single-Channel Molecular Conductor. *Nano Lett.* **2011**, *11*, 3734−3738.
(29) Bunte, S. W.; Jensen, G. M.; McNesby, K. L.; Goodin, D. B.; Chabalowski, C. F.; Nieminen, R. M.; Suhai, S.; Jalkanen, K. J. Theoretical Determination of the Vibrational Absorption and Raman Spectra of 3-Methylindole and 3-Methylindole Radicals. *Chem. Phys.* **2001**, *265*, 13−25.
(30) Aubard, J.; M'Bossa, C.; Bertigny, J. P.; Dubest, R.; Levi, G.; Boshet, E.; Guglielmetti, R. Surface Enhanced Raman Spectroscopy of Photochromic Spiroxazines and Related Spiropyrans. *Mol. Cryst. Liq. Cryst. Sci. Technol., Sect. A* **1994**, *246*, 275−278.
(31) Vasilyuk, G. T.; Maskevich, S. A.; Podtynchenko, S. G.; Stepuro, V. I.; Luk'yanov, B. S.; Alekseenko, Y. S. Structural Thermo- and Phototransformations of Oxaindane Spiropyrans Adsorbed on Silver Films. *J. Appl. Spectrosc.* **2002**, *69*, 344−350.
(32) Schneider, S.; Grau, H.; Ringer, J. Surface-Enhanced Resonance Raman Studies of Spiropyrans (Bips and Derivatives). *Mol. Cryst. Liq. Cryst. Sci. Technol., Sect. A* **1994**, *246*, 267−274.
(33) Li, Y.; Kaneko, S.; Fujii, S.; Kiguchi, M. Symmetry of Single Hydrogen Molecular Junction with Au, Ag, and Cu Electrodes. *J. Phys. Chem. C* **2015**, *119*, 19143−19148.
(34) Gu, C.; Wang, H.; Sun, H.; Liao, J.; Hou, S.; Guo, X. Origin and Mechanism Analysis of Asymmetric Current Fluctuations in Single-Molecule Junctions. *RSC Adv.* **2018**, *8*, 39408−39413.
(35) Gupta, A. K.; Hsu, C.-H.; Lai, C.-S. Enhancement of the Au/Zno-Na Plasmonic SERS Signal Using Principal Component Analysis as a Machine Learning Approach. *IEEE Photonics J.* **2020**, *12*, 1−11.
(36) Kamińska, A.; Witkowska, E.; Kowalska, A.; Skoczyńska, A.; Ronkiewicz, P.; Szymborski, T.; Waluk, J. Rapid Detection and Identification of Bacterial Meningitis Pathogens in Ex Vivo Clinical Samples by SERS Method and Principal Component Analysis. *Anal. Methods* **2016**, *8*, 4521−4529.
(37) Connolly, J. M.; Davies, K.; Kazakeviciute, A.; Wheatley, A. M.; Dockery, P.; Keogh, I.; Olivo, M. Non-Invasive and Label-Free Detection of Oral Squamous Cell Carcinoma Using Saliva Surface-Enhanced Raman Spectroscopy and Multivariate Analysis. *Nanomedicine* **2016**, *12*, 1593−1601.
(38) Zou, S.; Hou, M.; Li, J.; Ma, L.; Zhang, Z. Semi-Quantitative Analysis of Multiple Chemical Mixtures in Solution at Trace Level by Surface-Enhanced Raman Scattering. *Sci. Rep.* **2017**, *7*, No. 6186.
(39) He, X.; Liu, Y.; Huang, S.; Liu, Y.; Pu, X.; Xu, T. Raman Spectroscopy Coupled with Principal Component Analysis to Quantitatively Analyze Four Crystallographic Phases of Explosive Cl-20. *RSC Adv.* **2018**, *8*, 23348−23352.

https://doi.org/10.1021/acsomega.1c07105
ACS Omega 2022, 7, 5578−5583